

Research on Theoretical Model of Combined Micro-Machining of Laser and Electrolysis of Thermal Barrier Coated Turbine Blade Film Cooling Holes

Aixi Sun¹, Yulan Hu^{2,*} and Bo Hao^{1,3}

¹ School of Mechanical Engineering, Nanjing University of Science and Technology, Nanjing 210094, China

² School of Information Science and Engineering, Shenyang Ligong University, Shenyang 110159, China

³ School of Mechanical Engineering, Shenyang Ligong University, Shenyang 110159, China

*E-mail: wghao95@126.com

Received: 17 May 2016 / *Accepted:* 6 September 2016 / *Published:* 10 October 2016

In view of high quality machining demand of thermal barrier coated turbine blade film cooling holes, a new method of combined micro-machining of laser and electrolysis is presented in this thesis. First of all, in electrolyte fluid, micro-holes on thermal barrier coatings are milled by photochemical etching of ultraviolet laser. Moreover, micro-holes on nickel-based alloy blade are etched by high frequency pulsed electrochemical machining. It can manufacture film cooling holes by cold machining. No recast layer and micro-cracks are produced, so machining quality is improved. Meanwhile, the problem that conventional methods of electric machining such as electrochemical machining and electrical discharge machining can't etch non-conductive coatings is solved. Machining errors are reduced because only one single presetting cutter is needed from hole machining to its final shape. Methods like small clearance machining, side wall insulating tubular electrode and low concentration acidic electrolyte are applied in electrochemical machining to improve machining precision. This thesis analyzes photochemical etching conditions of micro-holes on thermal barrier coatings with ultraviolet laser, process of development and collapse of cavitation bubbles and their functions in laser machining. It puts forward mechanism of high frequency pulsed electrochemical machining of micro-holes on nickel-based alloy blade. And then, mechanism of combined micro-machining is researched. Heat conduction process in macroscopic materials of thermal barrier coatings and potential distribution in machining gap are analyzed by Fourier's law and Laplace Equation respectively. Cooling effects of electrolyte fluid in laser machining and influences of uneven distribution of electrolyte conductivity in electrochemical machining are considered. Theoretical model of combined micro-machining is established, the validity of which is proved by experiment.

Keywords: thermal barrier coatings; photochemical etching; film cooling holes; cold machining; theoretical model

1. INTRODUCTION

Micro-structures such as thermal barrier coated turbine blade film cooling holes determine the service life and reliability of parts. For instance, thermal load and mechanical load of turbine is the largest in aviation engine. Engine performance depends highly on inlet temperature of turbine, and it is limited by blade materials. So some new methodologies have to be adopted to achieve the high performance index. Technology of film cooling holes not only realizes effective cooling, but also controls aerodynamic losses caused by injection, turbulent flow and wall thermal stress concentration. Technology of thermal barrier coatings not only reduces surface temperature of hot end metal components, but also improve high temperature oxidation and corrosion resistance of matrix alloy. Film cooling holes are distributed mainly on the 3D surface of the blade and combustion chamber. Machining quality of holes including recast layer and micro-cracks directly determines the service life and stability of turbine blade. So they are micro-structure devices and are difficult to be machined.

In recent years, non-traditional machining technologies such as laser machining were more and more frequently applied to manufacturing technology of micro-structures. In micro-machining field of metallic materials like nickel-based alloys, electrochemical machining had the following advantages: good surface quality [1], high machining precision [2,3], no heat affected zone. However, it had problems existed, such as passivation, serious horizontal corrosion [4] and difficult exclusion of electrolysis products and so on. Electrical discharge machining had advantages such as no cutting force [5], good repeatability and controllability, but defects like low machining efficiency [6], thick recast layer [7], electrode loss [8] existed. Nanosecond laser machining with shorter wavelength [9] and laser machining under water immersion [10] effectively reduced heat affected zone. But recast layer was not eliminated. Composite micro-machining of laser and electrolysis efficiently removed recast layer in the hole wall, but recast layer was not also eliminated [11]. Laser drilling assisted with jet electrochemical machining effectively eliminated micro-cracks and recast layer thus improved machining surface quality. However, machining precision was reduced because jet scattered around the surface of workpiece produced stray corrosion [12]. Plus laser electrochemical machining removed passivation layer in a uniform electric field by the thermal-mechanical shock effect of laser local irradiation, and the material at this zone was etched. The other regional material was not removed, which enhanced the localisation of machining. However, serious attenuation of infrared laser in water led to too small laser energy and no thermal shock effect. Etching rate of material was very low and even was nil [13-14]. Femtosecond laser machining of directionally solidified superalloy and single crystal superalloy had recast layer and micro-cracks [15]. In micro-machining field of nonmetallic materials such as thermal barrier coatings, plasma impact force in picosecond laser machining generated micro-cracks of coating [16]. Femtosecond laser machining had advantages such as no thermal effect and high precision [17,18], however, its machining efficiency was much lower than nanosecond laser machining. Ultraviolet nanosecond laser machining of ceramics assisted with water had advantages such as no recast layer, high precision and high efficiency [19]. Conventional methods of electric machining such as electrochemical machining and electrical discharge machining did not machine insulating ceramic micro-structures. Electrical discharge machining [20] had heat affected zone and micro-cracks on machining region of ceramics by auxiliary electrode method.

Defects like recast layer and micro-cracks seriously affected the safety and reliability of thermal barrier coated turbine blade. Therefore, a new method of combined micro-machining of laser and electrolysis is presented in this thesis. First of all, in electrolyte fluid, micro-holes on thermal barrier coatings are milled by photochemical etching of ultraviolet laser. Moreover, micro-holes on nickel-based alloy blade are etched by high frequency pulsed electrochemical machining. It can manufacture film cooling holes by cold machining. No recast layer and micro-cracks are produced, so machining quality is improved. Meanwhile, the problem that conventional methods of electric machining such as electrochemical machining and electrical discharge machining can't etch non-conductive coatings is solved. Machining errors are reduced because only one single presetting cutter is needed from hole machining to its final shape. Methods like small clearance machining, side wall insulating tubular electrode and low concentration acidic electrolyte are applied in electrochemical machining to improve machining precision. It will provide technical support for micro-machining method of thermal barrier coated turbine blade film cooling holes with high quality and high precision.

This thesis analyzes photochemical etching conditions of micro-holes on thermal barrier coatings with ultraviolet laser, process of development and collapse of cavitation bubbles and their functions in laser machining. It puts forward mechanism of high frequency pulsed electrochemical machining of micro-holes on nickel-based alloy blade. And then, mechanism of combined micro-machining is researched. Heat conduction process in macroscopic materials of thermal barrier coatings and potential distribution in machining gap are analyzed by Fourier's law and Laplace Equation respectively. Cooling effects of electrolyte fluid in laser machining and influences of uneven distribution of electrolyte conductivity in electrochemical machining are considered. Theoretical model of combined micro-machining is established, the validity of which is proved by experiment.

2. MECHANISM OF COMBINED MICRO-MACHINING OF LASER AND ELECTROLYSIS OF THERMAL BARRIER COATED TURBINE BLADE FILM COOLING HOLES

Photochemical etching conditions of micro-holes on thermal barrier coatings with ultraviolet laser, process of development and collapse of cavitation bubbles and their functions in laser machining are analyzed. Mechanism of high frequency pulsed electrochemical machining of micro-holes on nickel-based alloy blade is put forward. And then, mechanism of combined micro-machining of laser and electrolysis is researched, which will provide foundation to establish theoretical model of combined micro-machining.

2.1 Ultraviolet laser machining mechanism of micro-holes on thermal barrier coatings assisted with electrolyte fluid

Photochemical etching conditions of micro-holes on thermal barrier coatings with ultraviolet laser are as follows. Single-photon excitation is shown in Figure 1(a). In thermal barrier coatings mainly containing zirconia doped by yttria, molecule bond energies of zirconia (about 4.5 eV) are larger than photon energies of ultraviolet laser (about 3.5 eV). Because the molecule bond cannot be directly destroyed by single-photon theoretically, so no photochemical reactions occur. However,

materials with wide band width have problems like the existence of doping and self-defect which will produce new energy band structures in bands where electrons cannot reside [21]. Electrons in ground state are excited into defect energy bands and have a short stay, and then, they leap into conduction band after absorbing the energy of second photon. Thereby, reaction of absorbing energies of more than two photons is multiphoton absorption. Only if pulse power density is larger than 10^6 W/cm^2 , electrons in ground state can simultaneously absorb two photons and leap into excited state, and obvious multiphoton absorption phenomena can occur [19]. Two-photon excitation is shown in Figure 1(b). In this thesis, power of ultraviolet laser is up to 15 W, spot diameter is about $40 \mu\text{m}$, pulse power density is up to $2.65 \times 10^9 \text{ W/cm}^2$. Therefore, multiphoton absorption conditions are satisfied.

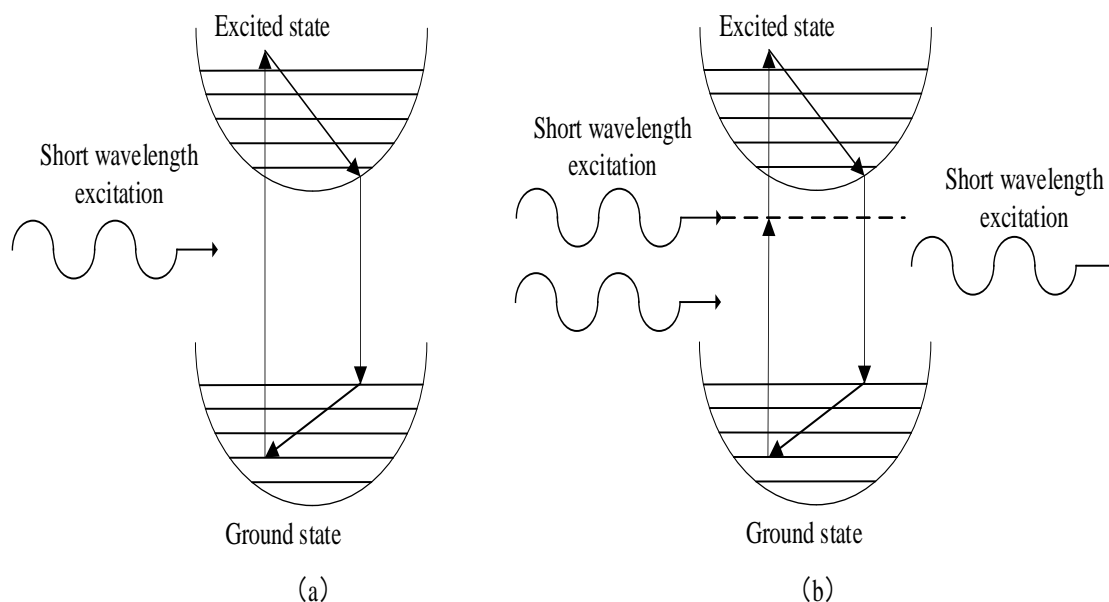


Figure 1. Single-photon excitation and two-photon excitation

Process of development and collapse of cavitation bubbles and their functions in laser machining are as follows[19,22]. When micro-holes on thermal barrier coatings are etched by ultraviolet laser in electrolyte, the collapse of cavitation bubbles produce jet impact force which is up to the magnitude of million Pa. Mechanism of jet impact force produced by cavitation bubbles is shown in Figure 2. Laser focuses on a point in liquid, light energy is transformed into thermal energy which vaporizes liquid, so cavitation bubbles are produced. Cavitation bubbles repeatedly expand and compress under difference between inner pressure and outer pressure, they finally collapse with the decrease of bubble energies and gas contents in bubbles. High pressure shock waves radiate outward and material matrices are acted on by intensive shocks, materials etched by laser are undocked quickly. So it can efficiently avoid the producing of recast layer.

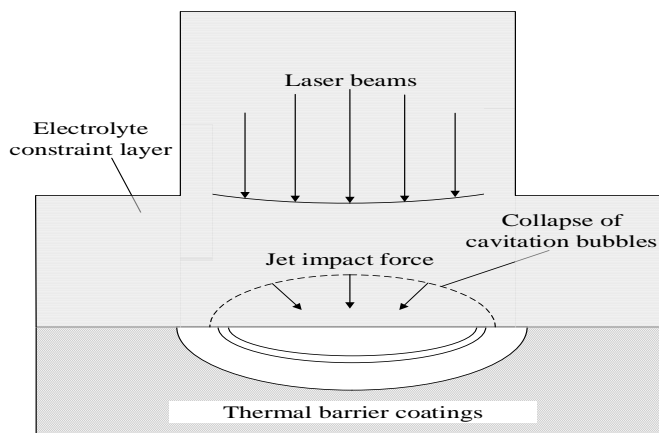


Figure 2. Mechanism of jet impact force produced by cavitation bubbles

2.2 Mechanism of high frequency pulsed electrochemical machining of micro-holes on nickel-based alloy blade based on small clearance

Based on electrochemical etching principles, mechanism of high frequency pulsed electrochemical machining of micro-holes on nickel-based alloy blade is researched.

Methods like small clearance (from 5 μ m to 15 μ m), side wall insulating tubular electrode and low concentration acidic electrolyte are applied in electrochemical machining. Mechanism of high frequency pulsed electrochemical machining of micro-holes on nickel-based alloy blade is shown in Figure 3 [23]. M indicates a metal in chemical composition of GH3030 nickel-based alloy workpiece, n is chemical valence of metal. Workpiece connects anode of electrolysis power, tubular electrode connects cathode of electrolysis power. A electric circuit is formed by workpiece, tubular electrode and mixed electrolyte (85g/L NaNO₃ and 2g/L NaHSO₄). Under the effect of electrolysis power, metal atoms in workpiece lost electrons and generate metal ions which dissolve in electrolyte. Hydronium ions on the end of electrode gain electrons, then generate hydrogen which release from electrolyte.

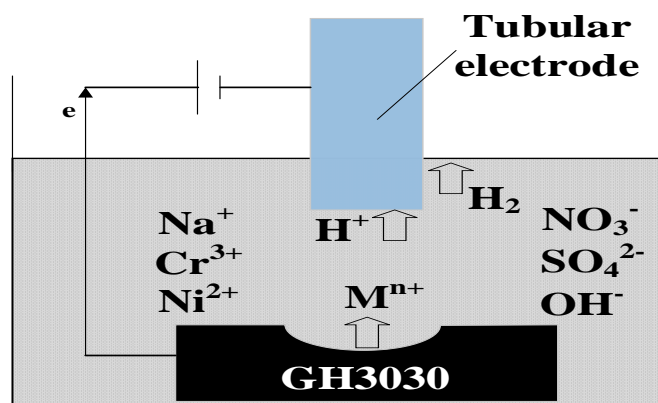
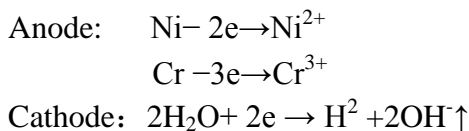


Figure 3. Mechanism of high frequency pulsed electrochemical machining of micro-holes on nickel-based alloy blade

Main chemical components of GH3030 nickel-based alloy are nickel and chromium. Formulas of electrochemical reaction of cathode and anode are as follow.



2.3 Mechanism of combined micro-machining of laser and electrolysis of thermal barrier coated turbine blade film cooling holes

Mechanism of combined micro-machining of laser and electrolysis of thermal barrier coated turbine blade film cooling holes is shown in Figure 4. First of all, rotary cutting method of nanosecond ultraviolet laser assisted with electrolyte fluid is applied. Photochemical effect is generated by multiphoton absorption, and micro-holes on thermal barrier coatings are milled. Meanwhile, shocks produced by the collapse of bubbles act on material matrices that can successfully prevent the secondary adhesion of etched materials. Moreover, small clearance machining, side wall insulating tubular electrode and low concentration acidic electrolyte are applied, micro-holes on nickel-based alloy blade are etched by high frequency pulsed electrochemical machining. Thereby, laser machining and electrochemical machining are realized in time of segmentation. Thermal barrier coated turbine blade film cooling holes without recast layer are achieved by cold machining. The precision and quality of machining is improved.

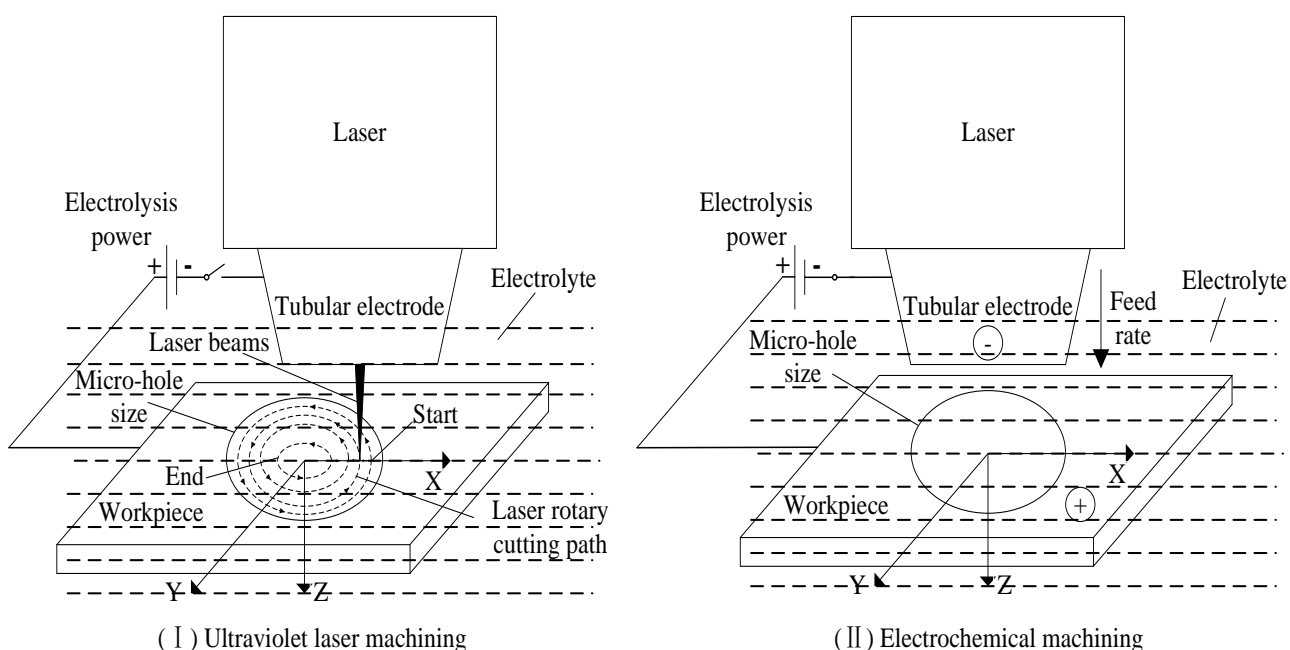


Figure 4. Mechanism of combined micro-machining of laser and electrolysis of thermal barrier coated turbine blade film cooling holes

3. THEORETICAL MODEL OF COMBINED MICRO-MACHINING OF LASER AND ELECTROLYSIS OF THERMAL BARRIER COATED TURBINE BLADE FILM COOLING HOLES

Cooling effects of electrolyte fluid in laser machining and influences of uneven distribution of electrolyte conductivity in electrochemical machining are considered. Theoretical model of combined micro-machining of laser and electrolysis is established. It can provide theoretical basis for establishment of experimental system of combined micro-machining process.

3.1 Model of ultraviolet laser machining of micro-holes on thermal barrier coatings assisted with electrolyte fluid

Heat conduction process in macroscopic materials of thermal barrier coatings is analyzed by Fourier's law. When ultraviolet laser irradiates thermal barrier coatings, electrons absorb laser energy on machining area, the temperature of which goes up. After temperature difference is produced between machining area and non-machining area, heat transfers from the warmest parts to the coldest parts in thermal barrier coatings.

In order to study temperature field distribution on the surface of thermal barrier coatings in electrolyte, the following assumptions are put forward [19, 24-27].

1) Nanosecond pulse laser is heat source which changes with time and space. Interaction between laser and electron-lattice system is ignored. The absorption of energy and the transformation of heat of macroscopic materials of thermal barrier coatings are considered.

2) The effect of defocus on spot size and laser power density is considered.

3) Molten materials of thermal barrier coatings are removed completely under the effect of shocks produced by the collapse of cavitation bubbles. It can successfully prevent the secondary adhesion of etched materials and the formation of recast layer.

4) In laser machining, the cooling effect of electrolyte fluid is considered, and the effect of plasma on absorption rate is ignored.

5) Materials of thermal barrier coatings are homogeneous mediums with isotropic properties, and physical thermal parameters of which are constant.

6) Production of chemical energy in machining and loss of energy by heating solution and thermal radiation are ignored.

Laser rotary cutting path in the XY plane is shown in Figure 5. Temperature field model of ultraviolet laser machining assisted with electrolyte fluid in the XZ plane is shown in Figure 6.

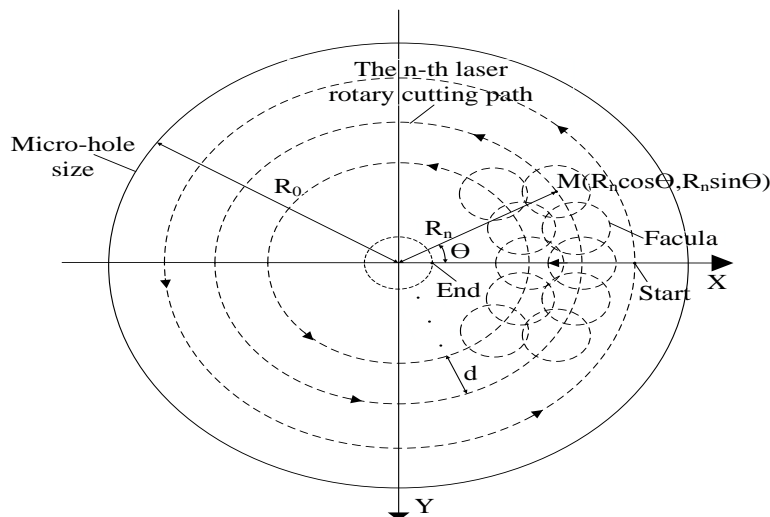


Figure 5. Laser rotary cutting path in the XY plane

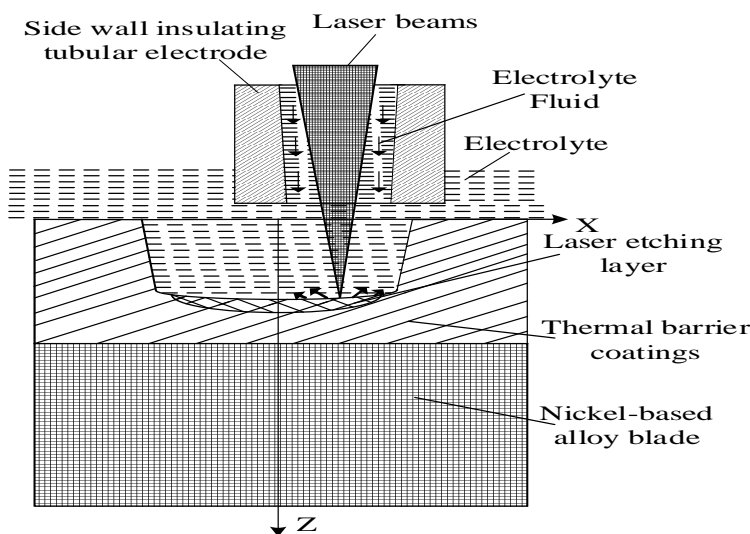


Figure 6. Temperature field model of ultraviolet laser machining assisted with electrolyte fluid in the XZ plane

Heat conduction process of materials of thermal barrier coatings on machining area submits Fourier's law. Three dimensional model of heat conduction equation is as follows [27,28].

$$\rho c \frac{\partial T(x, y, z, t)}{\partial t} = K \frac{\partial^2 T(x, y, z, t)}{\partial x^2} + K \frac{\partial^2 T(x, y, z, t)}{\partial y^2} + K \frac{\partial^2 T(x, y, z, t)}{\partial z^2} \quad (1)$$

The first boundary condition:

Initial temperature on machining range is as follows.

$$T(x, y, z, t = 0) = T_0 \quad (2)$$

The second boundary condition:

Heat flux density of ultraviolet laser on machining range is as follows [25-27].

$$q = A * \frac{Q}{\pi w(z - z_0)^2} * EXP(-\frac{(x - R_n \cos \theta)^2 + (y - R_n \sin \theta)^2}{w(z - z_0)^2}) * EXP(-u(\lambda)l) \quad (3)$$

In formula, $R_n = R_{n-1} - (n-1) * d$. $w(z - z_0)^2 = w_0^2 \left[1 + \left(\frac{\lambda(z - z_0)}{\pi w_0^2} \right)^2 \right]$. $\theta = \omega t$. R_n is laser rotary

cutting path radius. θ is laser rotary cutting angle. ω is laser rotary cutting angular speed. d is laser concentric circle rotary cutting spacing. $w(z - z_0)$ is faculae radius in z from beam waist. A is laser absorption rate of materials of thermal barrier coating. Q is laser pulse peak power. $\mu(\lambda)$ is attenuation coefficient of laser in electrolyte. l is laser transmission length in electrolyte.

The third boundary condition:

Convection heat transfer condition of electrolyte fluid on machining boundary of thermal barrier coatings is as follows [26, 27].

$$-K \frac{\partial T(x, y, z, t)}{\partial x} - K \frac{\partial T(x, y, z, t)}{\partial y} - K \frac{\partial T(x, y, z, t)}{\partial z} = h_c(T - T_0) \quad (4)$$

In formula, h_c is convection heat transfer coefficient of electrolyte fluid. T is surface temperature of thermal barrier coatings materials after laser machining. T_0 is initial temperature of electrolyte.

In ultraviolet laser machining, the pressure of electrolyte fluid on machining boundary of thermal barrier coatings approximately equals to inlet pressure of electrolyte. Change of convection heat transfer coefficient are caused by change of pressure of electrolyte fluid. So formula of convection heat transfer coefficient is as shown below [11,29].

$$h_c = \frac{K_{wat}}{L} Nu \quad (5)$$

In formula, $Nu = 0.7212 Pr^{0.37} Re^{0.5}$. K_{wat} is thermal conductivity of electrolyte. L is characteristic size of electrolyte fluid. Nu is Nusselt number of electrolyte. Pr is Prandtl number. Re is Reynolds number.

Temperature field distribution on the surface of thermal barrier coatings in single laser pulse duration is acquired by the above formulas and boundary conditions. Therefore, initial condition of next pulse laser machining is obtained by the removal of materials of thermal barrier coatings above melting point.

3.2 Electrochemical machining model of micro-holes on nickel-based alloy blade based on small clearance

3.2.1 Electric field model of electrochemical machining of micro-holes on nickel-based alloy blade

In order to study electric field distribution on the surface of nickel-based alloy blade, the following assumptions are put forward [26,30].

- 1) Because of axial symmetry of electrolyte fluid, two-dimensional XZ plane is analyzed.
- 2) Electric field of small clearance electrochemical machining is regarded as passive field and constant electric field.

3) The effect of gas-liquid two-phase flow on electrical conductivity of electrolyte in electrochemical machining is considered.

4) Electrochemical machining process of materials of nickel-based alloy blade obeys Faraday's law.

5) In machining, potential difference between cathode and anode approximately equals to decomposition voltage measured by experiment, which is constant.

Electric field model of electrochemical machining of micro-holes on nickel-based alloy blade in the XZ plane is shown in Figure 7.

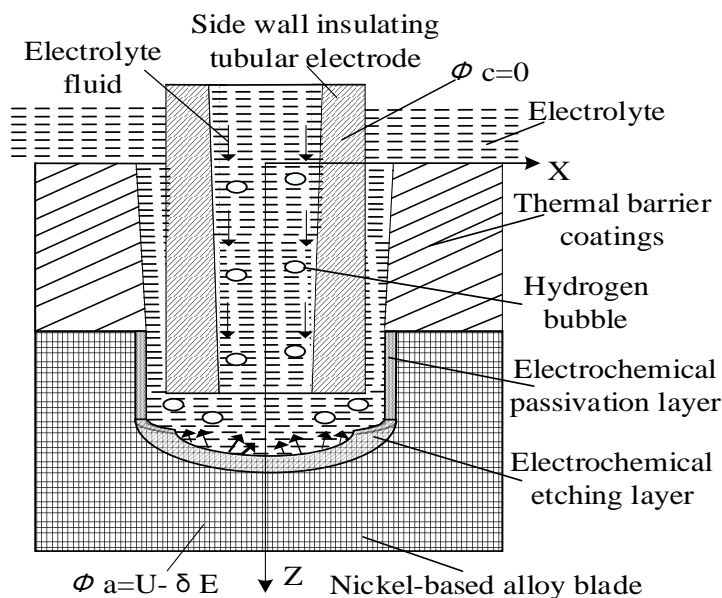


Figure 7. Electric field model of electrochemical machining of micro-holes on nickel-based alloy blade in the XZ plane

Electric potential distribution between tubular electrode and nickel-based alloy blade is corresponding to Laplace equation, which is as shown below.

$$\frac{\partial^2 \phi}{\partial x^2} + \frac{\partial^2 \phi}{\partial z^2} = 0 \tag{6}$$

Boundary condition of tubular electrode is as shown below.

$$\phi_c = 0 \tag{7}$$

Boundary condition of nickel-based alloy blade is as shown below.

$$\phi_a = U - \delta E \tag{8}$$

Material removal rate on machining boundary of nickel-based alloy blade is as shown below.

$$V_x = \eta \omega \kappa E_x \tag{9}$$

$$V_z = \eta \omega \kappa E_z \tag{10}$$

In formula, U is voltage between cathode and anode. δE is decomposition voltage. V is material removal rate. $\eta \omega$ is actual volume electrochemical equivalent. κ is electrical conductivity of electrolyte. E is electric field intensity.

Electric field distribution on the surface of nickel-based alloy blade in single pulse duration of electrochemical machining is obtained by the above formulas and boundary conditions. And then, material removal amount is acquired, initial condition of next pulse electrochemical machining is formed.

3.2.2 Flow field model of electrochemical machining of micro-holes on nickel-based alloy blade

In order to study flow field distribution on the surface of nickel-based alloy blade, the following assumptions are put forward [11,31].

- 1) Electrolyte fluid is incompressible and constant newtonian fluid, whose flow is constrained by mass conservation equation and momentum conservation equation.
- 2) Energy dissipation caused by change of medium temperature and temperature difference in machining is neglected.
- 3) The effect of low-Reynolds number is considered and the influence of gravity is ignored.

Flow field model of electrochemical machining of micro-holes on nickel-based alloy blade in the XZ plane is shown in Figure 8.

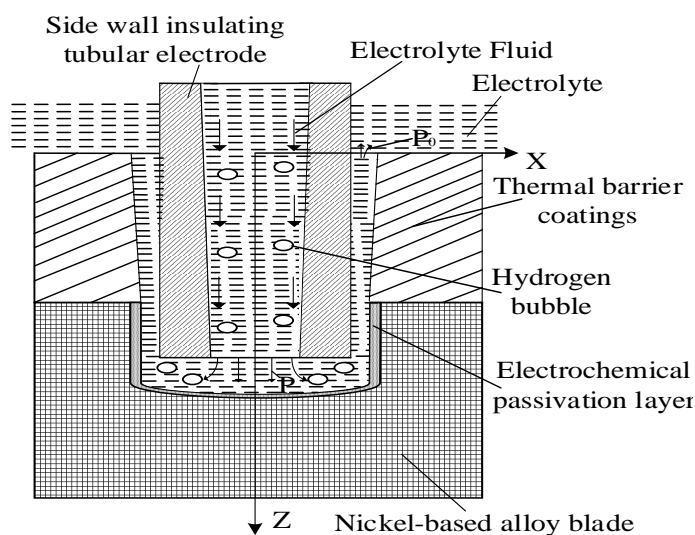


Figure 8. Flow field model of electrochemical machining of micro-holes on nickel-based alloy blade in the XZ plane

RNG k-ε turbulence model is used to analyze flow field distribution between tubular electrode and nickel-based alloy blade, which is as shown below [11,31].

$$\frac{\partial(\rho k)}{\partial t} + \frac{\partial(\rho k u_i)}{\partial x_i} = \frac{\partial}{\partial x_j} \left[\left(\mu + \frac{\mu_t}{\sigma_k} \right) \frac{\partial k}{\partial x_j} \right] + G_k - \rho \varepsilon \tag{11}$$

$$\frac{\partial(\rho \varepsilon)}{\partial t} + \frac{\partial(\rho \varepsilon u_i)}{\partial x_i} = \frac{\partial}{\partial x_j} \left[\left(\mu + \frac{\mu_t}{\sigma_\varepsilon} \right) \frac{\partial \varepsilon}{\partial x_j} \right] + \frac{C_{1\varepsilon}}{k} G_k - C_{2\varepsilon} \rho \frac{\varepsilon^2}{k} - R_\varepsilon$$

In formula, $R_\varepsilon = \frac{C_\mu \rho \eta^3 \left(1 - \frac{\eta}{\eta_0}\right) \varepsilon^2}{1 + \beta \eta^3} \cdot k$. k is turbulent kinetic energy. ε is dissipation rate of

turbulent kinetic energy. u_i is time-averaged velocity. μ_t is turbulent viscosity. G_k is the generation of turbulent kinetic energy caused by average velocity gradient.

Distribution of electrolyte pressure on the surface of nickel-based alloy blade in single pulse duration is acquired by the above formulas and boundary conditions.

3.2.3 Coupling relations of electric field and flow field of electrochemical machining of micro-holes on nickel-based alloy blade

Generated gases in electrochemical machining are distributed in electrolyte, so gas-liquid two-phase flow is produced and electrolyte conductivity is made to produce uneven distribution. Because the temperature of electrolyte is constant, formula of electrical conductivity of electrolyte is as shown below[11,30].

$$\kappa = \kappa_0 (1 - \beta)^{1.5} \quad (12)$$

In formula, $\beta = \frac{b_g R_g T |x|}{b_g R_g T |x| + \Delta_0 u_0 p}$. κ_0 is electrical conductivity at the inlet. β is bubble ratio.

b_g and R_g are constants. T is electrolyte temperature. Δ_0 is machining gap. u_0 is flow speed of electrolyte at the inlet. p is electrolyte pressure.

4. EXPERIMENTS OF COMBINED MICRO-MACHINING PROCESS

According to theoretical model of combined micro-machining, numerical simulative process of experimental system of combined micro-machining process was designed. The system was established by ANSYS parametric design language and the validity of theoretical model was proved by experiment.

4.1. Numerical simulative process of experimental system of combined micro-machining process

Numerical simulative process of experimental system of combined micro-machining process was shown in Figure 9. ANSYS parametric design language was applied to establish experimental system of combined micro-machining process. Final machining profile of combined micro-machining was obtained by results of laser machining and electrochemical machining.

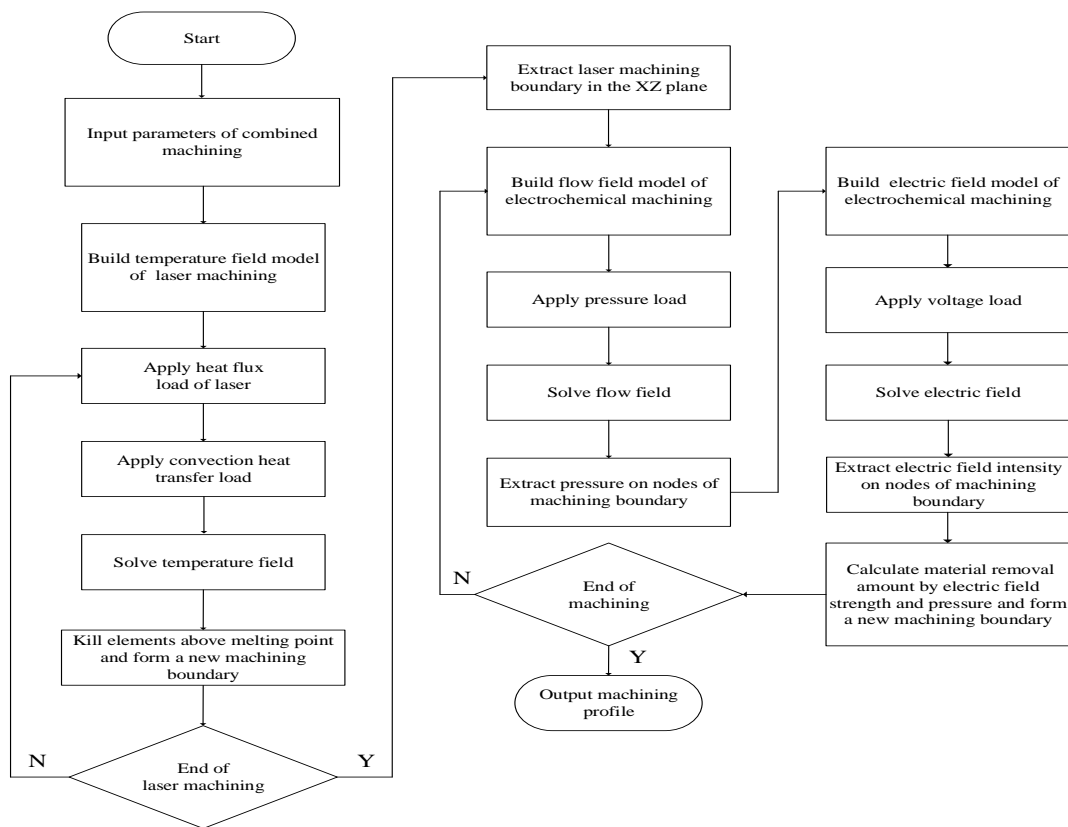


Figure 9. Numerical simulation process of experimental system of combined micro-machining process

4.2. Experimental verification of combined micro-machining process

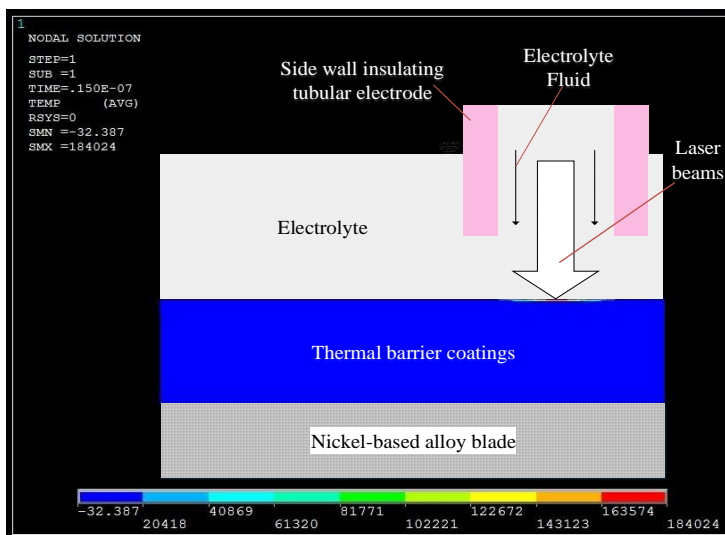


Figure 10. Temperature cloud chart on the surface of thermal barrier coatings in the first laser pulse duration in the XZ plane

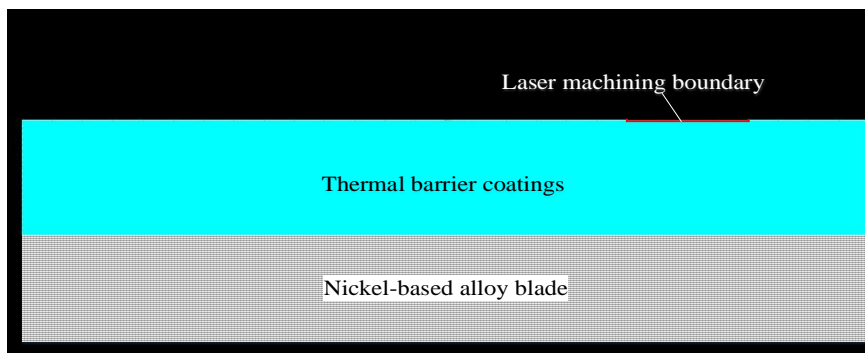
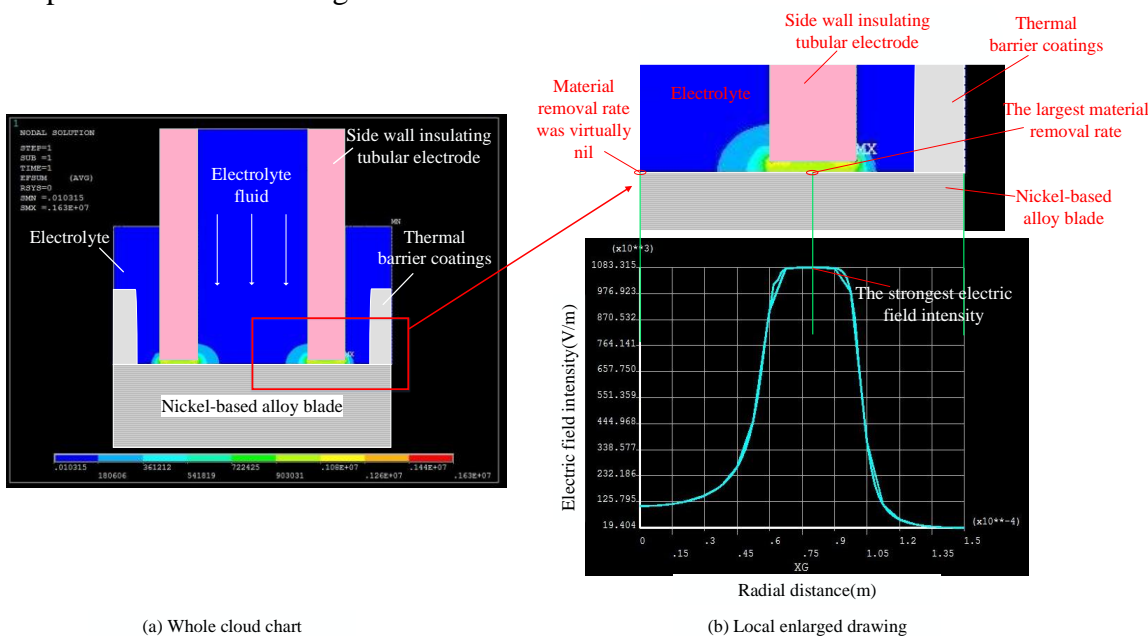


Figure 11. The boundary after the first laser pulse machining in the XZ plane

In ultraviolet laser machining assisted with electrolyte fluid, temperature field distribution on the surface of thermal barrier coatings was obtained by heat flux load of laser and convection heat transfer load. Temperature cloud chart on the surface of thermal barrier coatings was shown in Figure 10, which was machined by laser power with 7.515 W in the first laser pulse duration. Its center temperature reached up to 184024 °C. Therefore, after killing elements over melting point, initial boundary of next pulse laser machining was formed. The boundary after the first laser pulse machining in the XZ plane was shown in Figure 11.



(a) Whole cloud chart

(b) Local enlarged drawing

Figure 12. Electric field intensity cloud chart and radial electric field strength distribution diagram in first pulse duration of electrochemical machining in the XZ plane

Electric field intensity cloud chart and radial electric field strength distribution diagram on the surface of nickel-based alloy blade were shown in Figure 12, which was machined by 8 V electrolysis voltage in the first pulse duration of electrochemical machining. Material removal rate was obtained by electric field intensity, electrical conductivity and actual volume electrochemical equivalent. It was virtually nil on the center of micro-hole bottom. It increased with the increase of radial distance and was the largest on blade region corresponding to the center of electrode end. Also, it decreased with

the continued increase of radial distance. According to material removal rate and pulse width, initial boundary of next pulse electrochemical machining was obtained.

Process parameters of combined micro-machining of through-hole whose diameter was 0.2 mm were shown in Table 1. Other process parameters were as follows. Geometric scale of tubular electrode was 0.12 mm in internal diameter and was 0.2 mm in external diameter. The thickness of thermal barrier coated turbine blade materials was 0.65 mm and the thickness of ceramic thermal barrier coatings was 0.1 mm. Total machining time was 52 seconds and laser machining time was 6 seconds. Simulative results were as follows. Inlet diameter was 0.25 mm and outlet diameter was 0.241mm. Experimental results of combined micro-machining of through-hole were shown in Figure 13. Inlet diameter was 0.24 mm, outlet diameter was 0.236 mm. Simulative results were basically consistent with experimental results and met precision requirement ($\pm 0.05\text{mm}$), so the validity of theoretical model was proved by experiment.

Table 1. Process parameters of combined micro-machining of through-hole whose diameter was 0.2 mm

Process parameter of laser machining	Laser average power (W)	Laser pulse frequency (KHz)	Laser rotary cutting speed (mm/s)	Laser concentric circle rotary cutting spacing (μm)	Laser cutting depth (μm)	Electrolyte fluid pressure (Mpa)	Initial machining gap (mm)
	7.515	30	2.5	20	10	0.8	1.8
Process parameter of electrochemical machining	Electrode feed speed ($\mu\text{m/s}$)	Initial machining gap (μm)	Electrolysis voltage (V)	Duty cycle of pulse power	Frequency of pulse power (KHz)	Electrolyte fluid pressure (MPa)	
	12	6	8	0.5	12	0.2	

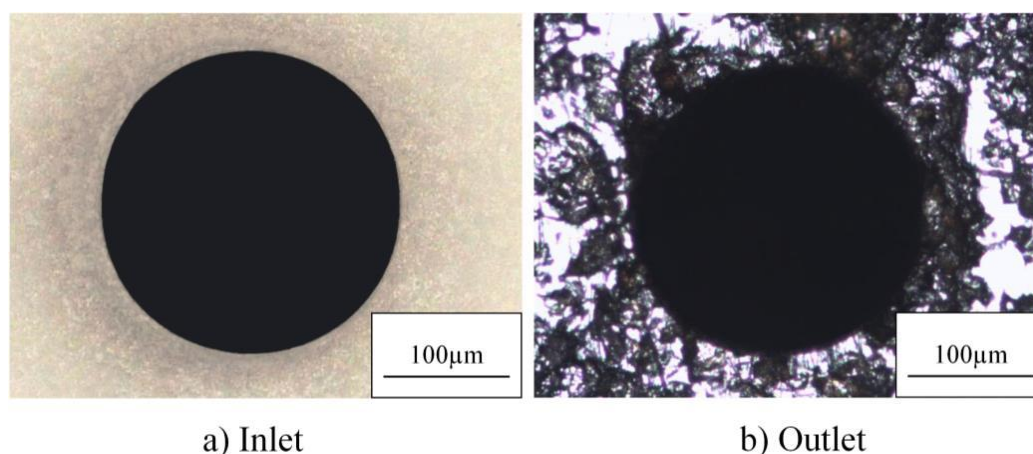


Figure 13. Experimental results of combined micro-machining of through-hole

Similar results and discussions were shown in Table 2. According to the knowledge of relevant theses, cooling effects of electrolyte fluid in laser machining and influences of uneven distribution of

electrolyte conductivity in electrochemical machining were considered. So simulative results were close to experimental results.

Table 2. Similar results and discussions

Classification	Name of thesis	Process parameters	Simulative result	Experimental result	Simulative error	Discussion
Laser machining	Study on UV laser microprocessing technology and mechanism for electronic materials [27]	Polyimide materials and 355 nm ultraviolet laser	40 μ m	39.4 μ m	0.6 μ m	The effect of convection between material and air was considered. Convection heat transfer coefficient was calculated. So the simulative result was close to the experimental result.
	Research on water-jet guided laser micromachining system and key technologies [29]	0Cr18Ni9 stainless steel and 1064 nm laser	128 μ m	118 μ m	10 μ m	The losses of heat transfer between materials and water jet and between materials and air were considered. Convection heat transfer coefficients between materials and water jet and between materials and air were calculated. So the simulative result was close to the experimental result.
Electrochemical machining	Study on system for simulation and prediction of workpiece's shape evolution by electrochemical machining [32]	2Cr13 stainless steel and electrolyte (the mass fraction of NaNO ₃ was 10 %)			0.1mm	The effect of bubbles produced in the process of electrochemical machining on results was not considered. Electrical conductivity of electrolyte at the inlet was used to calculate results of machining. So the simulative result was rather different from the experimental result.
	Research on experiment of NC-ECM with spherical cathode based on FEM [33]	1Cr18Ni9Ti stainless steel and electrolyte (the mass fraction of NaCl was 12 %)	0.30mm	0.35mm	0.05mm	The effect of gas-liquid two-phase flow on results in the process of electrochemical machining was not considered. So the simulative result was rather different from the experimental result.
	Research on the electric field characteristics of electrochemical machining with spherical cathode [34]	1Cr18Ni9Ti stainless steel and electrolyte (the mass fraction of NaCl was 12 %)	0.5mm	0.4mm	0.1mm	The effect of gas-liquid two-phase flow on results in the process of electrochemical machining was not considered. So the simulative result was rather different from the experimental result.
Combined machining	Basic research of hybrid processing of jet electro-chemical machining and laser	1Cr18Ni9Ti stainless steel, 532nm green laser and electrolyte (the mass			0.03mm	The precision of hybrid machining was determined by electrochemical machining. In simulating process of electrochemical machining, the effect of gas-liquid two-phase

machining [22]	fraction of NaNO ₃ was 18 %)				flow on results was not considered. So the simulative result was rather different from the experimental result.
Research on system and techniques of hybrid processing of laser beam machining with jet electrochemical machining [26]	1Cr18Ni9Ti stainless steel, 532nm green laser and electrolyte (the mass fraction of NaNO ₃ was 18%)			11μm	The precision of hybrid machining was determined by electrochemical machining. In simulating process of electrochemical machining, the effect of gas-liquid two-phase flow on results was not considered. So the simulative result was rather different from the experimental result.
Research on mathematical model of composite micromachining of laser and electrolysis based on the electrolyte fluid [11]	0Cr18Ni9 stainless steel and 532nm green laser	0.550mm	0.549mm	1μm	The precision of composite machining was determined by electrochemical machining. In simulating process of electrochemical machining, the effect of gas-liquid two-phase flow on results was considered. So the simulative result was close to the experimental result.
Research on the theoretical model of combined micro-machining of laser and electrolysis of thermal barrier coated turbine blade film cooling holes	Thermal barrier coatings mainly containing zirconia doped by yttria and ultraviolet laser GH3030 nickel-based alloy and mixed electrolyte (85g/L NaNO ₃ and 2g/L NaHSO ₄)	0.25mm	0.24mm	0.01mm	Cooling effects of electrolyte fluid in laser machining and influences of uneven distribution of electrolyte conductivity in electrochemical machining were considered. So simulative results were close to experimental results.
		0.241mm	0.236mm	0.005mm	

5. CONCLUSION

(1) A new method of combined micro-machining of laser and electrolysis is presented in this thesis. First of all, in electrolyte fluid, micro-holes on thermal barrier coatings are milled by photochemical etching of ultraviolet laser. Moreover, micro-holes on nickel-based alloy blade are etched by high frequency pulsed electrochemical machining. It can manufacture film cooling holes by cold machining. No recast layer and micro-cracks are produced, so machining quality is improved. It will provide technical support for micro-machining method of thermal barrier coated turbine blade film cooling holes with high quality.

(2) According to characteristics of combined micro-machining, photochemical etching conditions of micro-holes on thermal barrier coatings with ultraviolet laser, process of development and collapse of cavitation bubbles and their functions in laser machining are analyzed. Mechanism of high frequency pulsed electrochemical machining of micro-holes on nickel-based alloy blade is put

forward. And then, mechanism of combined micro-machining is researched, which will provide foundation to establish theoretical model of combined micro-machining.

(3) Heat conduction process in macroscopic materials of thermal barrier coatings and potential distribution in machining gap are analyzed by Fourier's law and Laplace Equation respectively. Cooling effects of electrolyte fluid in laser machining and influences of uneven distribution of electrolyte conductivity in electrochemical machining are considered. Theoretical model of combined micro-machining of laser and electrolysis of thermal barrier coated turbine blade film cooling holes is established. It can provide theoretical basis for establishment of experimental system of combined micro-machining process.

(4) According to theoretical model of combined micro-machining, ANSYS parametric design language is applied to establish experimental system of combined micro-machining process of laser and electrolysis. Simulative results are basically consistent with experimental results and meet precision requirement ($\pm 0.05\text{mm}$), so the validity of theoretical model is proved by experiment.

Conflict of Interests

The authors declare that they have no conflict of interests regarding the publication of this thesis.

ACKNOWLEDGMENTS

The work was supported by the National Natural Science Foundation of China (No. 61672360).

Reference

1. Xiuqing Fu, Min Kang, Yong Yang, MaoHua Xiao, *Journal of Machine Design*, 30 (2013) 11.
2. Zhaolong Li, Shichun Di, *Acta Armamentarii*, 33 (2012) 4.
3. Zhaoyan Zhang, Yaomin Wang, Fei Chen, Weipin Mao, *Journal of Nanjing University of Aeronautics & Astronautics*, 43 (2011) 1.
4. Hui Chen, Yukui Wang, Zhenlong Wang, Wansheng Zhao, *Nanotechnolog and Precision Engineering*, 9 (2011) 1.
5. Jiangtao Chen, Xijing Zhu, Jianqing Wang, Wenjun Kong, *Machine Tool and Hydraulics*, 42 (2014) 11.
6. Xiangzhi Wang, Zhidong Liu, Zheng Wei, Zongjun Tian, Yinhui Huang, *Journal of Nanjing University of Aeronautics & Astronautics*, 46 (2014) 5.
7. Zhiyong Cui, Zunyou Liu, Yi Wang, Meng Hu, Xiaohong Hao, *Mechanical Engineer*, (2013) 11.
8. Rongyuan Xue, Zhidong Liu, Xiangzhi Wang, Mingbo Qiu, Zongjun Tian, *China Mechanical Engineering*, 25 (2014) 9.
9. Hongkun Lai, Huan Qi, *Chinese Journal of Lasers*, 40 (2013) 8.
10. Abdulrehman M. Alahmari, Naveed Ahmed, Saied Darwish, *Int J Adv Manuf Technol*, (2015).
11. Aixi Sun, Bo Hao, Yulan Hu, Dewei Yang, *Mathematical Problems in Engineering*, 2016 (2016).
12. Lixin Yuan, Jiawen Xu, Jianshe Zao, Binghui Li, *Journal of Southeast University*, 40 (2010) 4.
13. Zhaoyang Zhang, Changliang Qin, Qinyu Feng, Yongbin Zeng, Mingxia Cai, Weiping Mao, Chun Su, *Journal of Mechanical Engineering*, 50(2014)23.
14. Zhaoyang Zhang, Changliang Qin, Qinyu Feng, Jie Yin, Weiping Mao, *Mechanical Science and Technology for Aerospace Engineering*, 34 (2015) 7.
15. Xinlin Liu, Chunhu Tao, Chunjiang Liu, Chunyan Hu, Xing Chen, *Materials Review*, 27 (2013) 11.

16. Ruifeng Sun, Xiaobing Zhang, Wenbin Cao, Shuili Gong, Xiaopeng Zhang, *Rare Metal Materials and Engineering*, 43 (2014) 5.
17. Junzhan Zhang, Yuqian Wang, Yin Zhang, Yongsheng Liu, *Optics and Precision Engineering*, 23 (2015) 6.
18. Tao Jiang, Qingfian Zhao, Rongwei Fan, Zhiwei Dong, Xin Yu, Weibo Li, *Infrared and Laser Engineering*, 41 (2012) 2.
19. Lingrui Kong, Fei Zhang, Jun Duan, Ruifeng Luo, Xiaoyan Zeng, *Laser Technology*, 38 (2014) 3.
20. Yongfeng Guo, Guowei Zhang, Li Wang, Yehui Hu, *Int J Adv Manuf Technol*, 83 (2016).
21. Brannon J.H., Lankard J.R., Baise A. I., Burns F., kaufman J., *Journal of Applied Physics*, 58 (1985) 5.
22. Hua Zhang, *Ph.D. Thesis of Nanjing University of Aeronautics & Astronautics*, (2009).
23. Yong Liu, *Ph.D. Thesis of Nanjing University of Aeronautics and Astronautics*, (2010).
24. Peng Gong, *M.S. Thesis of Jiangsu University*, (2013).
25. Zhiqiang Yun, *M.S. Thesis of Nankai University*, (2013).
26. Lixin Yuan, *Ph.D. Thesis of Nanjing University of Aeronautics and Astronautics*, (2013).
27. Fei Zhang, *Ph.D. Thesis of Huazhong University of Science and Technology*, (2012).
28. Zhaomei Xu, Yongzhi Liu, Jianzhong Zhou, Suqin Jiang, Qin'an Wang, Tongyue Wang, Zonghai Hong, *Infrared and Laser Engineering*, 43 (2014) 6.
29. Chunqi Li. *Ph.D. Thesis of Harbin Institute of Technology*, (2012).
30. Jiawen Xu, Naizhang Yun, Jianye Wang, Ji'an Tian, Wenyi Xu, *National Defense Industry Press*, (2008).
31. Xiuqing Fu, Min Kang, Yong Yang, Zexiang Liu, *China Mechanical Engineering*, 24 (2013) 8.
32. Lei Wang. *Modern Manufacturing Engineering*, (2010) 1.
33. Deying Liu, Xiuqing Fu, Min Kang, Chaopan Dong. *China Mechanical Engineering*, 24 (2013) 6.
34. Guoqian Liu, Xiuqin Fu, Min Kang, Chuan Liu, Jianing Wang, Changzhi Wang. *Proceedings of the 15th National Symposium on Special Processing*, (2013).